

# Dirac fermions at the $H$ point of graphite: Magneto-transmission studies

M. Orlita,<sup>1,2,3,\*</sup> C. Faugeras,<sup>1</sup> G. Martinez,<sup>1</sup> D. K. Maude,<sup>1</sup> M. L. Sadowski,<sup>1</sup> and M. Potemski<sup>1</sup>

<sup>1</sup>Grenoble High Magnetic Field Laboratory, CNRS, BP 166, F-38042 Grenoble Cedex 09, France

<sup>2</sup>Institute of Physics, Charles University, Ke Karlovu 5, CZ-121 16 Praha 2, Czech Republic

<sup>3</sup>Institute of Physics, v.v.i., ASCR, Cukrovarnická 10, CZ-162 53 Praha 6, Czech Republic

(Dated: October 30, 2018)

We report on far infrared (FIR) magneto-transmission measurements on a thin graphite sample prepared by exfoliation of highly oriented pyrolytic graphite (HOPG). In magnetic field, absorption lines exhibiting a blue-shift proportional to  $\sqrt{B}$  are observed. This is a fingerprint for massless Dirac holes at the  $H$  point in bulk graphite. The Fermi velocity is found to be  $\tilde{c} = (1.02 \pm 0.02) \times 10^6$  m/s and the pseudogap  $|\Delta|$  at the  $H$  point is estimated to be below 10 meV. Although the holes behave to a first approximation as a strictly 2D gas of Dirac fermions, the full 3D band structure has to be taken into account to explain all the observed spectral features.

PACS numbers: 71.70.Di, 76.40.+b, 78.30.-j, 81.05.Uw

The fabrication of graphene, a 2D lattice of carbon atoms with a honeycomb symmetry, and the subsequent discovery of Dirac fermions [1, 2, 3, 4], has led to renewed interest in the physical properties of bulk graphite. Compared to graphene, graphite represents a system of a higher complexity which is still not fully understood despite fifty years of intensive research. The currently accepted tight binding (TB) model, formulated for graphite by Slonzewski, Weiss and McClure (SWM) [5, 6], implies seven TB parameters  $\gamma_0, \dots, \gamma_5, \Delta$  and predicts the presence of particles with parabolic and linear dispersions at the  $K$  and  $H$  points of the Brillouin zone respectively. Whereas the appearance of massive electrons at the  $K$  point has been reported in numerous experiments, see e.g. [7, 8, 9], there is little direct evidence for Dirac fermions (holes) at the  $H$  point.

Evidence for  $\sqrt{B}$ -dependent features in magneto-reflectance spectra, typical for Dirac particles, has been reported by Toy *et al.* [10]. Recently, quantum oscillations in the magnetoresistance of bulk graphite [11, 12], indicated the presence of strictly 2D gases of both Dirac holes and massive electrons. Nevertheless, this interpretation remains controversial [13, 14] and raises some doubts concerning the accuracy of the SWM model. Further evidence of Dirac fermions close to the  $H$  point was obtained from angle resolved photoemission spectroscopy (ARPES) [15, 16]. However, the ARPES measurements gave differing Fermi velocities, information on the band structure only below the Fermi level, and are characterized by a rather low accuracy. Dirac holes have recently been observed in scanning tunneling spectroscopy (STS) [17], indicating again the pronounced 2D behavior of particles in HOPG. However, these investigations are principally limited to the surface of the sample and it is not understood why these effects have not been observed in equivalent experiments performed earlier [18].

In this Letter, we use FIR magneto-transmission experiments to probe the nature of the holes at the  $H$  point of HOPG. We address the currently controversial issue

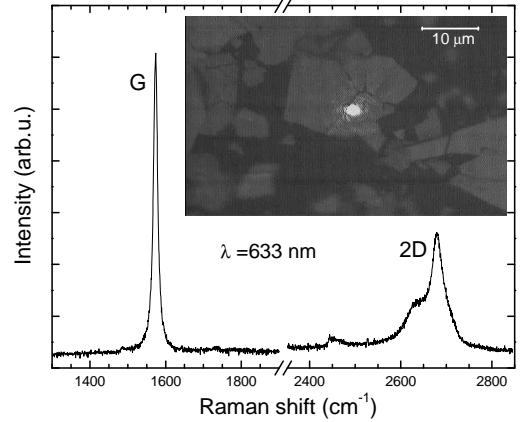


FIG. 1: A Raman spectrum of the studied sample showing the Raman bands  $G$  and  $2D$  typical of bulk graphite [19]. The bright laser spot in the middle of the microscope image in the inset shows the place, where this spectrum was collected.

of whether the holes in HOPG can be described using a simplified model assuming a strictly 2D gas of Dirac fermions as proposed in Refs. [11, 12, 17], or whether a full 3D band structure needs to be employed. We show that the appealing 2D model is in the simplest approach applicable, but simultaneously, we demonstrate the clear limits of this approximation. In this work, we focus on transitions, the energies of which scale as  $\sqrt{B}$ . However, in a different spectral region (low energies and high magnetic fields) we clearly observe features linear in  $B$ , which in accordance to previous reports [9] arise from electronic transitions in the vicinity of the  $K$  point.

A thin sample for the transmission measurements was prepared by exfoliation of HOPG. A confocal microscope image of part of the sample, i.e. of the tape with stacked graphite layers, is shown in the inset of Fig. 1. Scanning across the sample in the micro-Raman experiment, see Fig. 1, we only detected the signal typical of bulk graphite [19]. This signal corresponds to the light areas

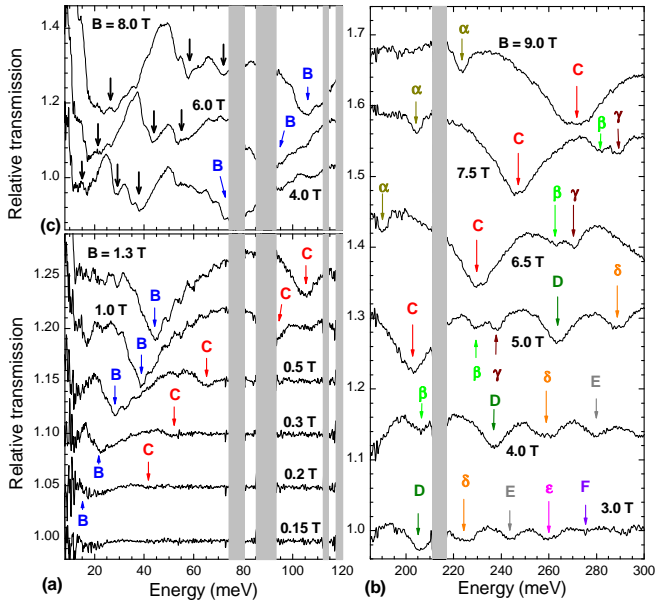


FIG. 2: (color online) Transmission spectra at selected magnetic fields in the low (a),(c) and high (b) energy windows. The lines denoted by individual letters exhibit a  $\sqrt{B}$ -scaled blue shift and are related to the  $H$  point. The low-energy features in (c), nearly linear in  $B$ , originate from the  $K$  point. The black arrows in (c) denote the most developed transmission minima whose positions were plotted into the inset of Fig. 3. For clarity, successive spectra in (a),(b) and (c) are shifted vertically by 0.05, 0.15 and 0.15, respectively.

in the picture, whereas the other dark areas (tape) exhibited no graphite or graphene signal. The layers of the bulk graphite of various thickness cover roughly 50% of the tape surface. The transmission experiment was performed on a macroscopic round-shaped sample having 5 mm in diameter. The average thickness of the graphite layers,  $\simeq 100$  nm, was roughly estimated from the transmissivity of the sample in the visible range.

The FIR experiments have been performed using the experimental setup described in Ref. [20]. To measure the transmittance of the sample, the radiation of global, delivered via light-pipe optics to the sample and detected by a Si bolometer, placed directly below the sample and cooled down to a temperature of 2 K, was analyzed by a Fourier transform spectrometer. All measurements were performed in the Faraday configuration with the magnetic field applied along the  $c$ -axis of the sample. All the spectra were taken with non-polarized light in the spectral range of 10-300 meV, limited further by several regions of low tape transmissivity (see gray areas in Figs. 2 and 3). The transmission spectra were normalized by the transmission of the tape and by the zero-field transmission, thus correcting for magnetic field induced variations in the response of the bolometer.

Typical spectra, characteristic of a number of samples prepared in the same way, are depicted in Fig. 2. Sev-

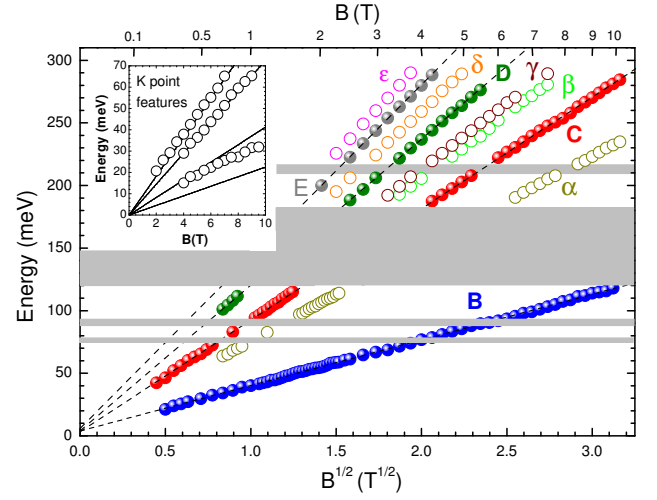


FIG. 3: (color online) Positions of absorption lines related to the  $H$  point as a function of  $\sqrt{B}$ . The dashed lines represent a least squares fit. Inset:  $K$  point related transmission minima showing a nearly linear with  $B$  dependence, as compared to the most prominent transitions (solid lines with slopes 2.3, 4.1, 7.3 and 9.1 meV/T) anticipated after Ref. [9]. The lowest observed minimum is broad and can be composed of two lines.

eral absorption lines showing a  $\sqrt{B}$ -dependence of their energies are observed in the spectra, as seen in Fig. 3. We relate these transitions to the  $H$  point of graphite. The dominant lines in the spectra are denoted by capital letters. The energies of the subsequent lines B to E scale as  $1 : (\sqrt{2} + 1) : (\sqrt{3} + \sqrt{2}) : (2 + \sqrt{3})$ . The integral intensities of these lines increase with the magnetic field. The widths of the absorption lines also increase, see e.g. the C line in Fig. 2, whose width increases from  $\approx 10$  meV at  $B = 1.3$  T to more than 30 meV at  $B = 9.0$  T. Weaker intensity features, which form a second series of absorption lines, are denoted by Greek letters. In addition, features which shift linearly with  $B$ , originating from the  $K$  point of graphite, are also observed in our spectra, see Fig. 2c. These features, which have already been reported in magneto-reflectivity data [9], are not further discussed in this work. The weak intensity modulation of spectra (visible in Fig. 2a,c above  $B \approx 0.5$  T), which does not shift with changing magnetic field, is attributed to interference effects in the sample.

To interpret  $\sqrt{B}$ -dependent features in our FIR spectra, we sketch the simplified SWM model of Landau levels (LLs) in the vicinity of the  $H$  point [6, 10]. Starting with four  $\pi$ -bands,  $E_1, E_2$  and the doubly degenerate  $E_3$ , we obtain four LLs for each index  $n \geq 1$  at a finite magnetic field  $B$ . In addition, we obtain three levels and one level for  $n = 0$  and  $n = -1$ , respectively. In the following, we use the notation  $E_1^n, E_2^n$  for  $n \geq 0$ ,  $E_{3+}^n, E_{3-}^n$  for  $n \geq 1$ ,  $E_3^0$  and  $E_3^{-1}$  to emphasize the band profile of the individual LLs. To distinguish among levels in Fig. 4, gray color is used for LLs  $E_1^n$  and  $E_2^n$ . The assumption

of zero trigonal warping ( $\gamma_3 = 0$ ) [6, 10] simplifies the eigenvalue problem to the diagonalization of  $4 \times 4$  matrices. At  $k_z = 0.5$ , we obtain the analytical solution  $E_3^0 = \Delta$ ,  $E_3^{-1} = 0$  and for  $n \geq 1$ :

$$E_{3\pm}^n = E_{1,2}^{n-1} = \frac{\Delta}{2} \pm \sqrt{\frac{\Delta^2}{4} + \xi B n}, \quad (1)$$

where “+” and “-” correspond to  $E_1^{n-1}$  and  $E_2^{n-1}$ , respectively, and  $\xi$  is related to  $\gamma_0$  via the expression  $\xi = 3\gamma_0^2 e a_0^2 / (2\hbar)$ , with  $a_0 = 0.246$  nm [21].

The selection rules for dipole-allowed interband transitions at  $k_z = 0.5$  predict the absorption lines at energies [10] ( $n \geq 1$ ):

$$\hbar\omega_n = \sqrt{\frac{\Delta^2}{4} + \xi B n} + \sqrt{\frac{\Delta^2}{4} + \xi B (n+1)}, \quad (2)$$

which correspond to transitions  $E_{3-}^n \rightarrow E_{3+}^{n+1}$  together with  $E_2^{n-1} \rightarrow E_1^n$  and, due to the expected electron-hole symmetry, also to transitions  $E_{3+}^{n-1} \rightarrow E_{3-}^n$  and  $E_2^n \rightarrow E_1^{n-1}$ . In addition to interband transitions, two dipole-allowed intraband transitions  $E_2^0 \rightarrow E_3^{-1}$  ( $\hbar\omega_{-1}$ ) and  $E_{3-}^1 \rightarrow E_3^0$  ( $\hbar\omega_0$ ), split in energy by  $\Delta$ ,

$$\hbar\omega_0 = \hbar\omega_{-1} + \Delta = \frac{\Delta}{2} + \sqrt{\frac{\Delta^2}{4} + \xi B}, \quad (3)$$

were experimentally found and discussed in Ref. [10].

A number of dipole-allowed transitions expected at  $k_z = 0.5$  are shown on the right-hand side of Fig. 4 by vertical solid arrows. Following the general assumption that the Fermi energy at the  $H$  point is negative, in Fig. 4 we assign the calculated lines to the experimentally observed lines, using the same notation by capital letters B, C, D, E and F as in Fig. 2. It is important to note that a non-zero value for the parameter  $\Delta$  implies the splitting of the strongest B transition into two  $B_0$  and  $B_{-1}$  components. However, this splitting is not resolved in the experiment. The upper limit of the pseudogap,  $|\Delta| < 10$  meV, estimated from the measured width of the B line is in a good agreement with Ref. [10], but in an apparent contradiction to Ref. [9] and recent theoretical calculations in Ref. [16]. In Fig. 4, we have used  $\Delta = -5.0$  meV. The clear observation of the B line, which accurately scales as  $\sqrt{B}$  down to  $B \approx 0.3$  T, allows us to estimate a Fermi energy,  $E_F \approx -20$  meV, in accordance with generally accepted values, see e.g [13], but somewhat smaller than the ARPES result ( $E_F \approx -50$  meV) [15].

Another important feature of our data is the clearly asymmetric shape of the B line as well as the significant line broadening with increasing magnetic field. We presume that both these effects indicate some contribution of the transitions at  $k_z \neq 0.5$  to the observed transmission spectra. At low magnetic field, the  $k_z$ -dispersion in the vicinity of the  $H$  point is steeper for  $E_2^0$  than for  $E_{3-}^1$  and this qualitatively explains the low field asymmetry. The

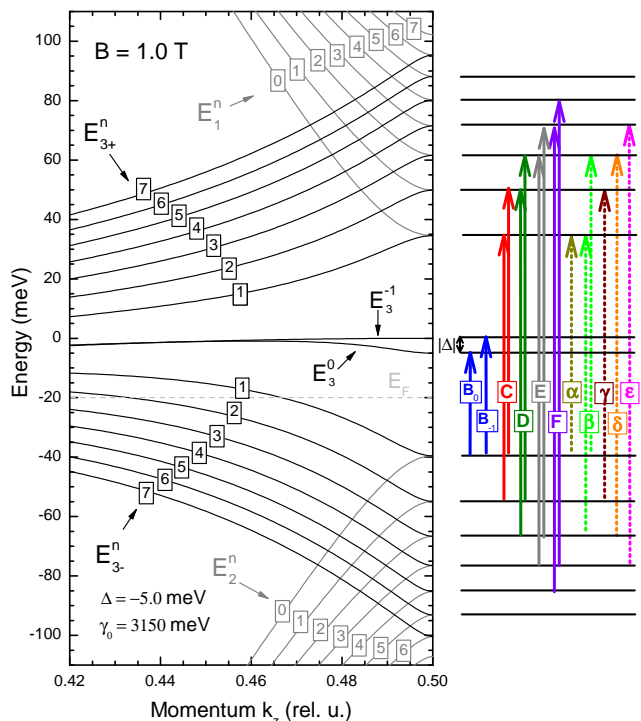


FIG. 4: (color online) LLs in graphite from  $n = -1$  to 7 as a function of momentum  $k_z$  in the vicinity of the  $H$  point ( $k_z = 0.5$ ) at  $B = 1.0$  T calculated using the SWM model neglecting trigonal warping ( $\gamma_3 = 0$ ). The arrows on the right-hand side show transitions considered in our interpretation. Except for  $\gamma_0$  and  $\Delta$ , the TB parameters used in the calculation were taken from Ref. [13].

dispersions become more symmetric with increasing  $B$ , as does the line shape of the B line. Nevertheless, the dispersions of all levels are steeper at higher magnetic fields, which qualitatively accounts for the broadening of the absorption lines. However, the agreement remains only qualitative. An additional mechanism for the line broadening is electron scattering probability, which increases linearly when moving away from the Dirac point [22]. Summing over the transitions for different momenta  $k_z$ , in terms of a simple calculation of the joint density of states, does not help to reproduce the spectral shapes of the observed lines. Some additional  $k_z$  dependent selection rules, enhancing the oscillator strength in the close vicinity of  $k_z = 0.5$  point need to be introduced.

The relatively small value of the pseudogap  $\Delta$  is consistent with the very good linearity of data with  $\sqrt{B}$  (see Fig. 3). The limit of  $\Delta \rightarrow 0$  allows us to rewrite Eq. (1) as  $E_{3\pm}^n = E_{1,2}^{n-1} = \pm\sqrt{\xi B n}$ , which has the form of LLs in a 2D system of massless Dirac fermions. The energies of the dipole-allowed transitions (2),(3) can then be for  $n \geq 0$  written as  $\hbar\omega_n = \sqrt{\xi B}(\sqrt{n} + \sqrt{n+1})$  and a clear correspondence to the optical transitions in graphene is established [20, 23]. The Fermi velocity can then be expressed in the form  $\tilde{c} = \sqrt{\xi/(2e\hbar)}$  and from our data

evaluated to be  $\tilde{c} = (1.02 \pm 0.02) \times 10^6$  m/s, which is about 10% higher than in [15] but in a good agreement with the most recent data [16, 17]. We stress that the entire fan chart of the observed inter LL transitions reported here can be described with a single parameter (Fermi velocity). This is a surprising observation, as Kohn's theorem is not expected to hold in a system with a strongly non parabolic one particle dispersion, so that electron-electron interaction may differently alter excitations between different pairs of LLs. Note that the linear fits in Fig. 3 extrapolate to an onset  $\approx 3$  meV instead of zero, which possibly suggests, apart from the anticrossing splitting  $\Delta$ , an additional mutual shift of the electron and hole Dirac cones, however, this effect lies on the edge of the experimental accuracy.

We turn now our attention to the additional transitions, denoted in Figs. 2 and 3 by Greek letters, which are in general of a lower intensity. They exhibit a clear  $\sqrt{B}$ -dependence and have no counterpart in the transmission spectra of graphene [20, 24]. To interpret these lines we have to go beyond the simplified model used in [6, 10] and consider a more complete analysis [25]. The selection rules  $n \rightarrow n \pm 1$  ( $n \geq 1$ ) is predicted not only for the main transitions  $E_{3-}^n \rightarrow E_{3+}^{n\pm 1}$  and  $E_2^n \rightarrow E_1^{n\pm 1}$ , but also for a second series of lines, presumably weaker in intensity,  $E_{3-}^n \rightarrow E_1^{n\pm 1}$  and  $E_2^n \rightarrow E_{3+}^{n\pm 1}$ . We can then relate the absorption lines  $\alpha, \gamma, \delta$  and  $\epsilon$  to transitions which are symmetric with respect to the Dirac point, as depicted in Fig. 4 by the vertical dotted arrows. In agreement with expectations, the energies of these lines scale as  $1 : \sqrt{2} : \sqrt{3} : 2$  and the same Fermi velocity is derived ( $\tilde{c} = (1.02 \pm 0.02) \times 10^6$  m/s) as for the main transitions.

Another series of weak absorption lines, predicted in [25], should satisfy the selection rules  $n \rightarrow n \pm 2$ . Their oscillator strength is directly connected to the parameter  $\gamma_3$ . The  $\beta$  line can then be assigned to transitions  $E_{3-}^{3(1)} \rightarrow E_{3+}^{1(3)}$  and/or  $E_2^{2(0)} \rightarrow E_1^{0(2)}$ , representing thus a direct indication of the trigonal warping in graphite, demonstrated experimentally e.g. in [15, 16].

Having interpreted all observed absorption lines, we can draw the following conclusions. The dominant transitions in the spectra, which have their counterpart in the spectra of graphene [20, 24], justify that holes in HOPG can, with a reasonable accuracy, be described as a purely 2D gas of Dirac fermions. This justifies the model adopted for interpreting STS experiments [17] and quantum oscillations in graphite [11, 12]. Nevertheless, the latter analysis is not consistent with our data, when estimating the hole density. Whereas in our experiment, the hole filling factor  $\nu = 6$  is achieved at  $B \approx 0.3$  T, when the B line clearly appears in the spectrum, the same value of  $\nu$  is found at magnetic fields above 1 T in the magnetotransport data [11, 12].

On the other hand, the series of additional absorption lines of weaker intensity, which are dipole-forbidden in the strictly 2D gas of Dirac particles, show that in

HOPG we are dealing with a strongly anisotropic but nevertheless 3D system and the model of a purely 2D gas is not valid in general. The 3D nature of graphite is also shown by the pronounced low field asymmetry of the B line and possibly by the observed increase in linewidth with increasing  $B$ .

In summary, FIR magneto-transmission measurements have been used to probe the Dirac holes at the  $H$  point in a thin graphite layer prepared by the exfoliation of HOPG. We find a relatively small value for the pseudo-gap  $|\Delta| < 10$  meV, consistent with the observation of Dirac fermions at the  $H$  point of graphite, with a Fermi velocity of  $\tilde{c} = (1.02 \pm 0.02) \times 10^6$  m/s. The main absorption lines can be understood using a model which assumes a strictly 2D gas of Dirac fermions, giving evidence for the strong anisotropy of HOPG. Nevertheless, the presence of additional weaker transitions, dipole-forbidden in a purely 2D system of Dirac fermions, can only be understood by considering the 3D nature of graphite.

The present work was supported by the European Commission through Grant No. RITA-CT-2003-505474, by contract ANR-06-NANO-019 and projects MSM0021620834 and KAN400100652.

---

\* Electronic address: orlita@karlov.mff.cuni.cz

- [1] K. S. Novoselov, A. K. Geim, S. Morozov, D. Jiang, M. I. Katsnelson, I. Grigorieva, S. Dubonos, and A. A. Firsov, *Science* **306**, 666 (2004).
- [2] C. Berger, Z. Song, T. Li, X. Li, A. Y. Ogbazghi, R. Feng, Z. Dai, A. N. Marchenkov, E. H. Conrad, P. N. First, et al., *J. Phys. Chem. B* **108**, 19912 (2004).
- [3] K. S. Novoselov, A. K. Geim, S. V. Morozov, D. Jiang, M. I. Katsnelson, I. V. Grigorieva, S. V. Dubonos, and A. A. Firsov, *Nature* **438**, 197 (2005).
- [4] Y. B. Zhang, Y. W. Tan, H. L. Stormer, and P. Kim, *Nature* **438**, 201 (2005).
- [5] J. C. Slonczewski and P. R. Weiss, *Phys. Rev.* **109**, 272 (1958).
- [6] J. W. McClure, *Phys. Rev.* **119**, 606 (1960).
- [7] J. K. Galt, W. A. Yager, and H. W. Dail, Jr., *Phys. Rev.* **103**, 1586 (1956).
- [8] P. R. Schroeder, M. S. Dresselhaus, and A. Javan, *Phys. Rev. Lett.* **20**, 1292 (1970).
- [9] Z. Q. Li, S.-W. Tsai, W. J. Padilla, S. V. Dordevic, K. S. Burch, Y. J. Wang, and D. N. Basov, *Phys. Rev. B* **74**, 195404 (2006).
- [10] W. W. Toy, M. S. Dresselhaus, and G. Dresselhaus, *Phys. Rev. B* **15**, 4077 (1977).
- [11] I. A. Luk'yanchuk and Y. Kopelevich, *Phys. Rev. Lett.* **93**, 166402 (2004).
- [12] I. A. Luk'yanchuk and Y. Kopelevich, *Phys. Rev. Lett.* **97**, 256801 (2006).
- [13] G. P. Mikitik and Y. V. Sharlai, *Phys. Rev. B* **73**, 235112 (2006).
- [14] B. A. Bernevig, T. L. Hughes, S. Raghu, and D. P. Arovas, *Phys. Rev. Lett.* **99**, 146804 (2007).
- [15] S. Y. Zhou, G.-H. Gweon, J. Graf, A. V. Fedorov, C. D.

- Spataru, R. D. Diehl, Y. Kopelevich, D.-H. Lee, S. G. Louie, and A. Lanzara, *Nature Phys.* **2**, 595 (2006).
- [16] A. Grüneis, C. Attaccalite, T. Pichler, V. Zabolotnyy, H. Shiozawa, S. Molodtsov, D. Inosov, A. Koitzsch, M. Knupfer, J. Schiessling, et al., *Phys. Rev. Lett.* **100**, 037601 (2008).
- [17] G. Li and E. Andrei, *Nature Phys.* **3**, 623 (2007).
- [18] T. Matsui, H. Kambara, Y. Niimi, K. Tagami, M. Tsukada, and H. Fukuyama, *Phys. Rev. Lett.* **94**, 226403 (2005).
- [19] A. C. Ferrari, J. C. Meyer, V. Scardaci, C. Casiraghi, M. Lazzeri, F. Mauri, S. Piscanec, D. Jiang, K. S. Novoselov, S. Roth, et al., *Phys. Rev. Lett.* **97**, 187401 (2006).
- [20] M. L. Sadowski, G. Martinez, M. Potemski, C. Berger, and W. A. de Heer, *Phys. Rev. Lett.* **97**, 266405 (2006).
- [21] D. D. L. Chung, *J. Mater. Sci.* **8**, 1475 (2002).
- [22] Y. Zheng and T. Ando, *Phys. Rev. B* **65**, 245420 (2002).
- [23] V. P. Gusynin, S. G. Sharapov, and J. P. Carbotte, *Phys. Rev. Lett.* **98**, 157402 (2007).
- [24] Z. Jiang, E. A. Henriksen, L. C. Tung, Y.-J. Wang, M. E. Schwartz, M. Y. Han, P. Kim, and H. L. Stormer, *Phys. Rev. Lett.* **98**, 197403 (2007).
- [25] G. Dresselhaus and M. S. Dresselhaus, *Phys. Rev.* **140**, A401 (1965).